

See discussions, stats, and author profiles for this publication at: <https://www.researchgate.net/publication/235680715>

Vibrational and Electronic Structure Analysis of a Carbon Dioxide Interaction with Functionalized Single-Walled Carbon Nanotubes

ARTICLE in THE JOURNAL OF PHYSICAL CHEMISTRY A · MARCH 2013

Impact Factor: 2.69 · DOI: 10.1021/jp312622s · Source: PubMed

CITATIONS

5

READS

42

6 AUTHORS, INCLUDING:



Pedro Henrique de Oliveira Neto

University of Brasília

28 PUBLICATIONS 140 CITATIONS

[SEE PROFILE](#)



Geraldo Magela e Silva

University of Brasília

90 PUBLICATIONS 488 CITATIONS

[SEE PROFILE](#)



João B.L. Martins

University of Brasília

67 PUBLICATIONS 649 CITATIONS

[SEE PROFILE](#)



Ricardo Gargano

University of Brasília

101 PUBLICATIONS 587 CITATIONS

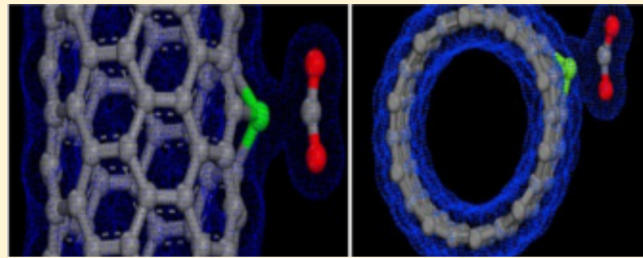
[SEE PROFILE](#)

Vibrational and Electronic Structure Analysis of a Carbon Dioxide Interaction with Functionalized Single-Walled Carbon Nanotubes

Edson Nunes Costa Paura, Wiliam F. da Cunha, Pedro H. de Oliveira Neto, Geraldo M. e Silva, Joao B. L. Martins, and Ricardo Gargano*

Institute of Physics, University of Brasilia

ABSTRACT: Electronic and vibrational properties of different single-walled carbon nanotubes (SWNTs) interacting with a CO₂ molecule are investigated through the use of density functional theory (DFT) calculations and the discrete variable representation (DVR) method, respectively. We observed a considerable geometry difference between pristine and doped nanotubes. Consequently, a greater binding energy between the former type of nanotubes and the adsorbing molecule is achieved, a fact that finds experimental support and leads us to consider cobalt-doped nanotubes as promising candidates for chemical sensors. From the vibrational point of view, we note that the zigzag chirality tends to present higher values of vibrational frequencies for most of the states considered regardless of the nanotubes being doped or not. The potential energy curves (PECs) for the interactions between CO₂ and all of the considered nanotubes together with spectroscopic constants are provided, and the reliability of the performed calculations makes the data a useful source of comparison for future works.



1. INTRODUCTION

It is a well-known that carbon dioxide (CO₂) plays a central role in the existence of life, for being a fundamental structure in the carbon cycle. The interaction of CO₂, water, and light provides the primary energy source for most of the living cells through the complex process of photosynthesis. Due to the importance of this phenomenon, this gas has long ago attracted the attention of the scientific community.^{1–3} The consequential technological effort developed in the investigation of its properties allowed the understanding of the CO₂ production as a result of coal and hydrocarbons combustion.⁴ The major industrial development observed in the last centuries has turned the CO₂ production into a severe environmental problem. The reason is that CO₂, besides being an important greenhouse gas contributing to global warming,⁵ is a considerable source of ocean acidification,⁶ thus affecting the very basis of the earth food chain. As many problems due to global warming and ocean acidification have already hit our planet, efforts to overcome these issues are of the greatest importance.

A key stage in attempting to solve these CO₂-related environmental problems is the accurate and reliable detection of this gas on a scale that allows mapping its concentration in any media. Among the candidates for gas detection in general, nanostructured materials stand out with great potential use because their large surface to volume ratio provides a high degree of sensibility to molecular adsorption. The SWNT, an interesting representative of the nanostructured material class, has been intensively studied both from the experimental and theoretical points of view.^{7–9} Although pristine SWNTs tend to be chemically inert, they exhibit the possibility of presenting high adsorption energy when doped.¹⁰ Due to this low

reactivity, SWNTs have been the object of little research in the field of CO₂ adsorption. An instructive example of this field of research lies in the work of Zhao et al. By using a local density approximation (LDA), the adsorption energies of several small gases, including CO₂, on SWNTs and bundles have been investigated.¹¹ They found adsorption energies as low as in the range of 2–2.5 kcal/mol on different SWNTs. In another work, Cinke and co-workers used small cluster models with a single benzene molecule as a surrogate for the carbons, thus simulating a whole nanotube.¹² It was found that SWNTs adsorb nearly twice as much CO₂ as an activated carbon with a similar surface area, and the interaction energy was found to be very sensitive to the size of the basis set used, so that these calculations do not adequately address the binding of CO₂ to a real nanotube. While these works have yielded small values of the binding energy for the pristine SWNT–CO₂ system, a recent theoretical result has shown the power of functionalization on promoting gas absorption in carbon nanotubes.¹³ Whereas a binding energy increase of several gases with transition-metal-doped SWNTs was reported, the particularly important description of the adsorption of CO₂ was not carried out. From the experimental point of view, Matranga et al. studied CO₂ trapped inside of SWNT bundles as a result of heating the nanotubes, causing the decomposition of oxygen-containing functional groups.¹⁴ They concluded that in the absorption processes, some sites are blocked for the CO₂ interaction. Another missing feature in the literature is the

Received: December 21, 2012

Revised: February 7, 2013

Published: February 20, 2013

investigation of the chirality effect, a parameter that is thought to alter thermodynamic properties of SWNTs and their band structure and consequently is believed to affect their reactivity, IR spectra, and so on.⁸ The idea of performing calculations with a CO₂ molecule was to contribute to novel data on this important subject rather than to carry out a comparative study with other molecules. Several studies have already reported the chemical interaction of CO₂ with cobalt and others transition metals^{15–18} from other points of view. Therefore, we used this system to study this interaction.

An analysis of the reported works leads us to the conclusion that the description of the CO₂ adsorption mechanism as well as the vibrational spectra of the system remains controversial. The kind of nanotube in terms of size, chirality, and doping should be considered. The present work is developed to investigate the influence of these characteristics over electronic and spectroscopic vibrational properties of the SWNT–CO₂ complex. We performed an extensive set of DFT calculations for geometries, electronic energies, spectroscopic constants, and vibrational shifts of CO₂ interacting with the external surfaces of armchair (SWNT(5,5) and (10,10)) and zigzag (SWNT-(10,10) and (17,0)) pristine and cobalt-doped carbon nanotubes. In all cases, we considered periodic boundary conditions along the principal nanotube axes in order to mimic a system of infinite length. Edge effects tend to create preferred regions along the nanotube, a fact that might induce the observation of effects of purely computational nature. The consideration of an infinite nanotube is desired to inhibit such effects and thus to simulate a system of actual physical and chemical properties.

This work is organized as follows: in section 2, we describe the main computational features together with the methods used; section 3 is used to present the main results and the description of our calculations; and we outline the conclusions in section 4.

2. METHODOLOGY

Electronic structure calculations were performed within density functional theory (DFT). The equilibrium geometry and binding energies were calculated by using the DMol³ package.¹⁹ In all of the SCF calculations, a double numerical basis including the d-polarization function (DND) was adopted. The density functional was treated by the local density approximation (LDA) with the exchange–correlation potential parametrized by Perdew and Wang.²⁰ Along the tube axis, 1 × 1 × 10 Monkhorst–Pack *k*-points were used for the Brillouin zone integration. The relaxed atomic structures of the tubes were obtained by minimization of the total energy using Hellmann–Feynman forces including Pullay-like corrections.

Following, we performed several single-point DFT calculations for varying distances between the CO₂ molecule and the considered SWNT. We thus obtained a set of points consisting of our PEC that we chose to fit in an analytical expression through the use of a extended Rydberg²¹ function of the type

$$V(R) = -D_e \left[1 + \sum_{k=1}^{n=10} c_k (R - R_e)^k \right] e^{-c_l(R - R_e)} \quad (1)$$

where D_e stands for dissociation energy, R_e for the equilibrium distance, both of which were fixed prior to the fittings, and c_k are the coefficients to be determined (in this work, they were obtained by Powell's method²²). It is important to note that, for R_e to be used, we have to establish different definitions for this equilibrium distance, depending on the system to be doped or

not. In this sense, R_e refers to the equilibrium distance between the carbon atom of the CO₂ molecule and the nearest hexagon center of the nanotube when a pristine system is considered and alternatively, between the carbon center of the CO₂ and the substitutional cobalt atom of the doped SWNT.

By fitting our electronic energy results with extended Rydberg functions (eq 1), we were able to obtain novel analytical expressions for the several considered systems to be used in the solution of the Schrödinger nuclear equation through the application of the DVR methodology²³ and, in this fashion, to obtain rovibrational energies $\mathcal{E}(v, J)$, where v and J , respectively, denote the vibrational and the rotational quantum numbers. From these energies, one can obtain rovibrational spectroscopic constants using the following equations²⁴

$$\begin{aligned} \omega_e &= \frac{1}{24} [14(\mathcal{E}_{1,0} - \mathcal{E}_{0,0}) - 93(\mathcal{E}_{2,0} - \mathcal{E}_{0,0}) \\ &\quad + 23(\mathcal{E}_{3,0} - \mathcal{E}_{1,0})] \\ \omega_e x_e &= \frac{1}{4} [13(\mathcal{E}_{1,0} - \mathcal{E}_{0,0}) - 11(\mathcal{E}_{2,0} - \mathcal{E}_{0,0}) \\ &\quad + 3(\mathcal{E}_{3,0} - \mathcal{E}_{1,0})] \\ \omega_e y_e &= \frac{1}{6} [3(\mathcal{E}_{1,0} - \mathcal{E}_{0,0}) - 3(\mathcal{E}_{2,0} - \mathcal{E}_{0,0}) \\ &\quad + (\mathcal{E}_{3,0} - \mathcal{E}_{1,0})] \\ \alpha_e &= \frac{1}{8} [-12(\mathcal{E}_{1,1} - \mathcal{E}_{0,1}) + 4(\mathcal{E}_{2,1} - \mathcal{E}_{0,1}) + 4\omega_e \\ &\quad - 23\omega_e y_e] \\ \gamma_e &= \frac{1}{4} [-2(\mathcal{E}_{1,1} - \mathcal{E}_{0,1}) + (\mathcal{E}_{2,1} - \mathcal{E}_{0,1}) + 2\omega_e x_e \\ &\quad - 9\omega_e y_e] \end{aligned} \quad (2)$$

3. RESULTS AND DISCUSSION

In order to study the interaction between carbon nanotubes and the CO₂ molecule, we considered SWNTs with zigzag (10,0) and (17,0) and armchair (5,5) and (10,10) chiralities. The goal was to investigate effects of the chirality, diameter, and the substitutional doping (a carbon was exchanged by a cobalt atom in the active site of the nanotube) on the binding energy and on the vibrational spectra of the SWNT–CO₂ complexes.

In order to do this, we started by fully optimizing the geometry of each nanotube and the CO₂ molecule through the use of the DMol³ package. Following, the structure of the tube and the C–O bond length of the CO₂ molecule were fixed, while the distance between the tube and the molecule was varied to obtain the system energy as a function of the separation (PECs). These energies were calculated from the following expression

$$E_b = -(E_{\text{dimer}} - E_{\text{SWNT}} - E_{\text{CO}_2})$$

where E_{dimer} , E_{SWNT} , and E_{CO_2} are the total energies of dimers, the pure nanotube, and the CO₂ molecule, respectively.

In the route of our study, the pristine carbon nanotubes and the CO₂ molecules were initially optimized separately. A total of 80 atoms to SWNT(5,5) and SWNT(10,0), 136 atoms to SWNT(17,0), and 160 atoms to SWNT(10,10) were considered. We obtained a C–C bond distance of approximately 1.42 Å for the nanotubes and a typical linear structure

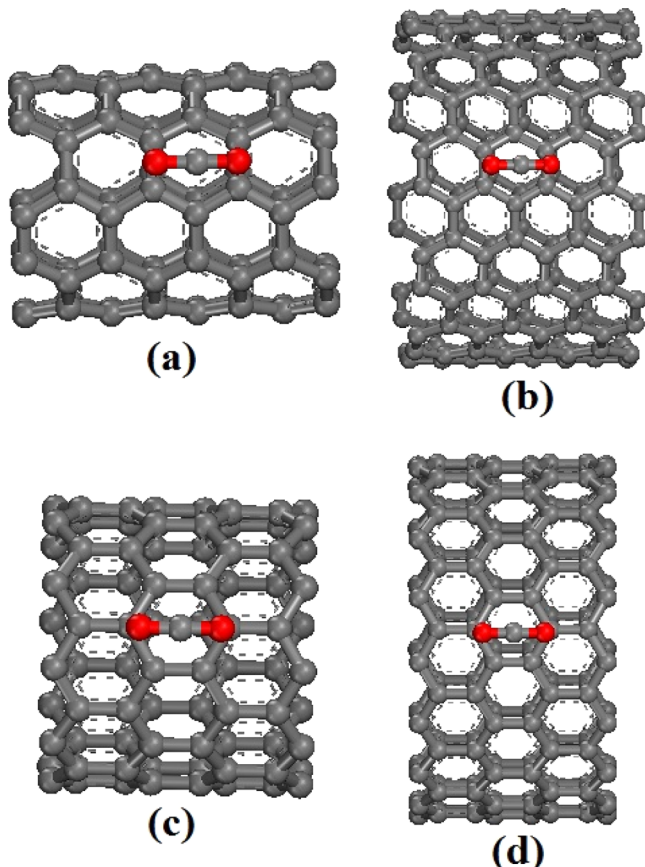


Figure 1. Equilibrium configuration of the CO₂ molecule related to the nanotubes: (a) SWNT(5,5), (b) SWNT(10,10), (c) SWNT(10,0), and (d) SWNT(17,0).

Table 1. Binding Energies and Equilibrium Distances for SWNT–CO₂ Dimers

chirality	carbon nanotube	binding energy (eV)	equilibrium distance (Å)
armchair	SWNT(5,5)	0.122	3.26
	SWNT(10,10)	0.124	3.15
zigzag	SWNT(10,0)	0.121	3.25
	SWNT(17,0)	0.125	3.20

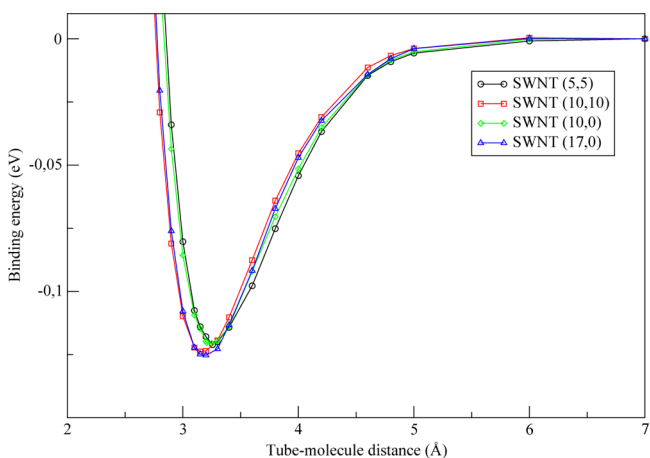


Figure 2. Comparison between the SWNT–CO₂ binding energy curves.

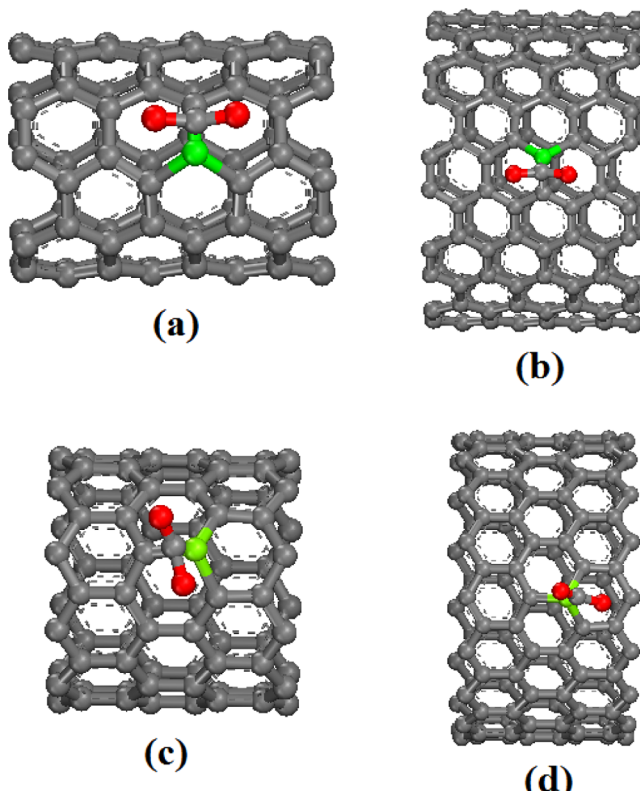


Figure 3. Equilibrium configuration of the CO₂ molecule related to the nanotubes doped with Co: (a) SWNT(5,5)@Co, (b) SWNT(10,10)@Co, (c) SWNT(10,0)@Co, and (d) SWNT(17,0)@Co.

Table 2. Binding Energy and Equilibrium Distance for SWNT@Co–CO₂ Complexes

chirality	cobalt doped carbon nanotube	binding energy (eV)	equilibrium distance (Å)
armchair	SWNT(5,5)@Co	0.642	2.01
	SWNT(10,10)@Co	0.713	2.01
zigzag	SWNT(10,0)@Co	1.120	2.02
	SWNT(17,0)@Co	1.075	2.02

for the CO₂, with a C–O bond distance of 1.166 Å, results that are in a good agreement with experimental data.⁷ This C–C distance is between the experimental sp²–sp² and sp–sp bond distances that are 1.47 and 1.37 Å, respectively. After that, the SWNT–CO₂ complexes were optimized to obtain the minimal configuration of each composed system. Figure 1 shows the equilibrium configuration of the CO₂ molecule related to the armchair and the zigzag nanotubes. It was observed that both the nanotube structure and the CO₂ molecule preserve their original structures.

An important feature that must be mentioned is that the complex minimal-energy configuration is obtained as the CO₂ carbon atom is located at the center of the hexagon surface of the nanotube, regardless of the chirality and diameter considered. This fact can be explained by noting that the carbon atom from the CO₂ molecule is able to fit exactly above the electronic density gap that once existed around the hexagon center.

Table 1 presents the equilibrium distances and binding energies of the SWNT–CO₂ interaction. From the obtained binding energy values, we concluded that the interactions can be considered as physisorption, being comparable to the

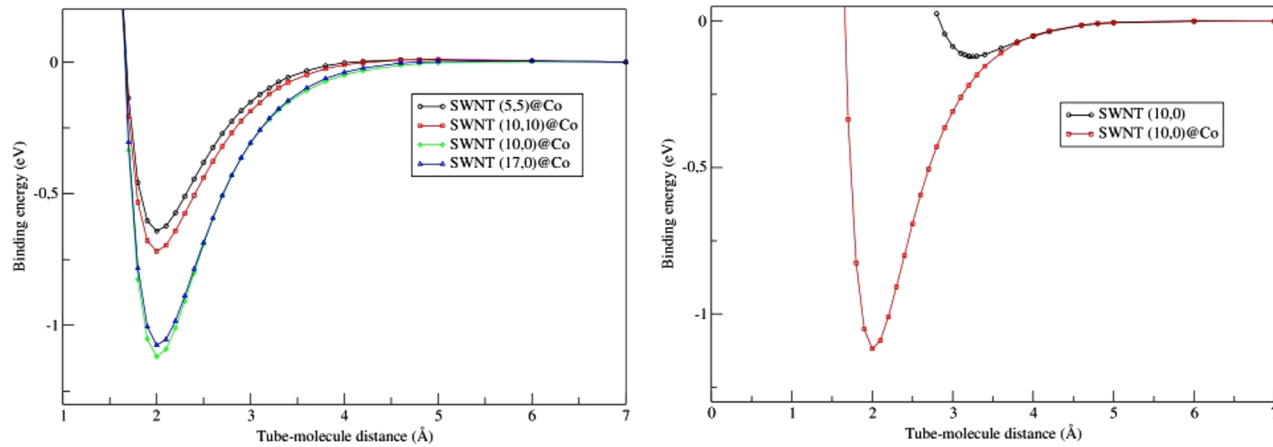


Figure 4. (a) Comparison between the SWNT@Co- CO_2 binding energy curves and (b) comparison between SWNT(10,0)- CO_2 and SWNT(10,0)@Co- CO_2 ones.

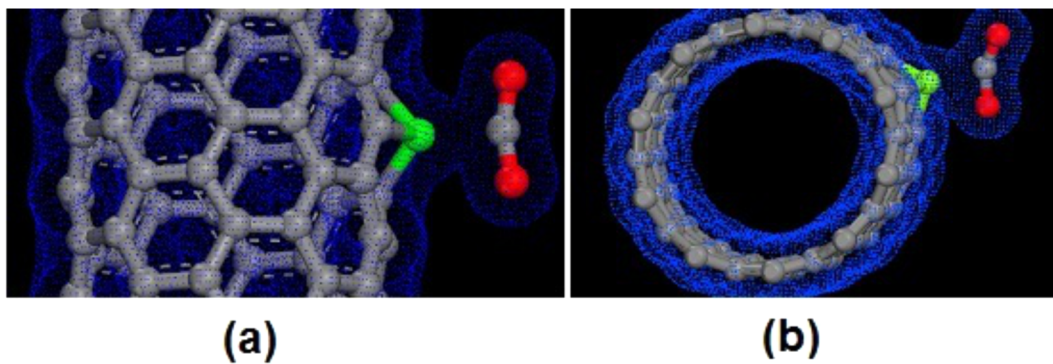


Figure 5. Density of charges: (a) SWNT(5,5)@Co- CO_2 and (b) SWNT(10,0)- CO_2 .

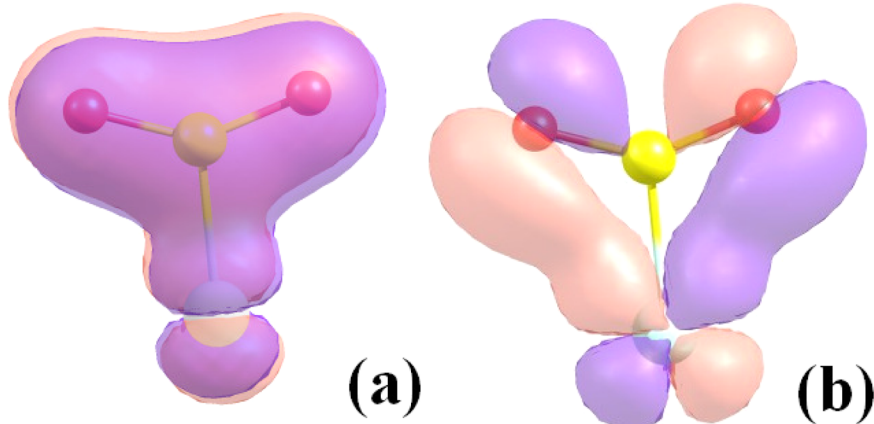


Figure 6. (a) σ and (b) π back-donation of CO_2 .

interaction between some molecules and a graphite surface.²⁵ These results indicate that in the case of pristine systems, one cannot trace a clear dependence between molecular adsorbent (CO_2) and the size and chirality of nanotubes.

Figure 2 shows the binding energy curves for the SWNT- CO_2 dimers. These curves were obtained by keeping the structure of the nanotube and the C–O bond lengths of the CO_2 molecule fixed, while the distance between the nanotube surface and the molecule was varied from the asymptotic region

until the strong interaction one. This result corroborates the conclusion that the SWNT- CO_2 binding energy is roughly independent of chirality and of the nanotube size.

The interaction of CO_2 molecule with cobalt-doped nanotubes (SWNT@Co) was studied using this same approach. In the present case, the SWNT geometry optimization was performed after the replacement of a carbon atom by one atom of cobalt. Figure 3 shows the SWNT@Co geometric configuration and the CO_2 molecule positioning

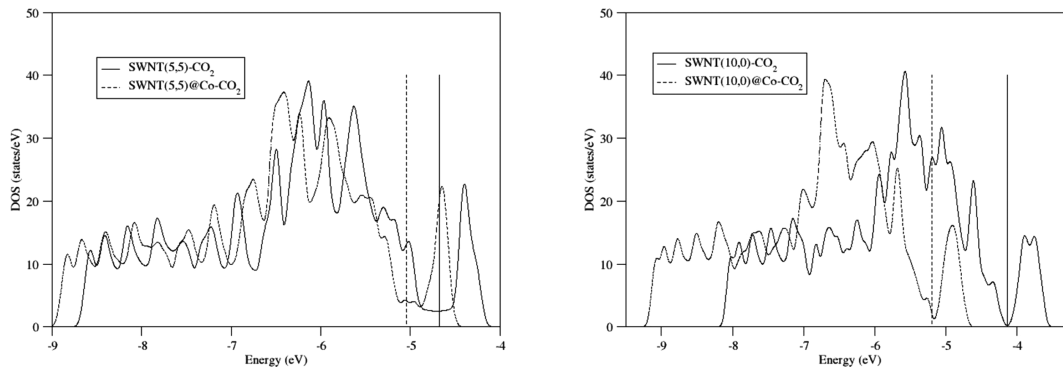


Figure 7. DOS of (a) a pristine (5,5) SWNT (solid curves) and the doped (dashed curves) systems and (b) a pristine (10,0) SWNT (solid curves) and doped (dashed curves) systems. The vertical solid and dotted lines denote the Fermi levels of the pristine and doped nanotube systems, respectively.

Table 3. Fitting Coefficients for the SWNT–CO₂ PECs

coefficients (\AA^{-k})	SWNT(5,5)	SWNT(10,10)	SWNT(10,0)	SWNT(17,0)
C_1	0.3915822×10	0.4664988×10	0.4772971×10	0.3467438×10
C_2	0.4614858×10	0.8039590×10	0.7875246×10	0.3219132×10
C_3	0.4709356×10	0.1140428×10^2	0.6341815×10	0.7432849
C_4	0.4842485×10	0.5764068×10	0.6667037×10	-0.2101869×10
C_5	-0.7738864×10	-0.2309872×10^2	0.1140877×10^2	0.2859279×10
C_6	-0.6013644×10	0.1304353×10^2	-0.2567284×10^2	0.3673018×10
C_7	0.1681224×10^2	0.4933516×10^2	-0.1221702×10^2	-0.1387300×10
C_8	-0.1106500×10^2	-0.6558933×10^2	0.9962090×10	-0.1398141×10
C_9	0.2923777×10	0.2886595×10^2	-0.2193531×10	0.8301816
C_{10}	-0.2413836	-0.4312851×10	$0.3457924 \cdot 10^{-1}$	-0.1161040

Table 4. Fitting Coefficients for the SWNT@Co–CO₂ PECs

coefficients (\AA^{-k})	SWNT(5,5)@Co	SWNT(10,10)@Co	SWNT(10,0)@Co	SWNT(17,0)@Co
C_1	0.4995970×10	0.4330407×10	0.5917578×10	0.5618396×10
C_2	0.8133241×10	0.5208141×10	0.1365741×10^2	0.1214293×10^2
C_3	0.9811145×10	0.4871221×10	0.2202264×10^2	0.2066881×10^2
C_4	0.8774630×10	0.4922771×10	0.2386244×10^2	0.2027173×10^2
C_5	-0.6184946×10	-0.2380810×10	-0.4095873×10	-0.2353505×10^2
C_6	0.2419269×10	-0.2217275×10	0.8147098×10	0.1856425×10^2
C_7	0.2721481×10^2	0.1239342×10^2	0.6348388×10^2	0.9841917×10^2
C_8	-0.3657031×10^2	-0.1348670×10^2	-0.5017603×10^2	-0.1295377×10^3
C_9	0.1948910×10^2	0.6099261×10	0.1788848×10^2	0.6746005×10^2
C_{10}	-0.4083351×10	-0.1065451×10	0.7862174	-0.1179863×10^2

Table 5. Vibrational Energies for the SWNT–O₂ and SWNT@Co–O₂ Dmers (values in parentheses)

ν	SWNT(5,5) (cm^{-1})	SWNT(10,10) (cm^{-1})	SWNT(10,0) (cm^{-1})	SWNT(17,0) (cm^{-1})
0	34.03(94.32)	33.34(96.74)	36.38(117.56)	33.24(111.03)
1	99.56(279.60)	98.12(287.18)	107.05(349.40)	98.90(329.04)
2	162.25(460.73)	161.98(473.53)	174.37(577.69)	163.39(543.32)
3	222.71(637.91)	224.82(655.94)	238.47(802.74)	226.54(754.61)
4	281.24(811.34)	286.37(834.51)	299.48(1024.75)	288.16(963.33)
5	338.03(981.14)	346.30(1009.34)	357.60(1243.87)	348.07(1169.71)
6	393.11(1147.41)	404.32(1180.52)	413.01(1460.16)	406.11(1373.85)
7	446.49(1310.25)	460.17(1348.15)	465.92(1673.68)	462.11(1575.78)
8	498.10(1469.70)	513.65(1512.31)	516.49(1884.42)	515.92(1775.47)
9	547.85(1625.81)	564.61(1673.06)	564.87(2092.39)	567.39(1972.86)
10	595.64(1778.62)	612.97(1830.47)	611.13(2297.54)	616.39(2167.88)

after the optimization. We observe a small increase in the C–C bond distance, from 1.42 Å (pristine system) to 1.44 Å. Another point that should be stressed is that the Co–C distance varies. It is 1.82 Å for armchair chirality, while this

value is 1.77 Å for zigzag chirality. This fact demonstrates that the cobalt atom is better accommodated by zigzag rather than by armchair nanotubes. Theoretical study of CO₂ adsorption on cobalt surfaces shows a distance between 1.89 and 2.23 Å,

Table 6. Vibrational Spectrum Shifts When the SWNT–CO₂ Dimers Are Transferred from Pristine to Doped SWNT–CO₂ (see text for discussion)

transitions (cm ⁻¹)	shift A	shift B	shift C	shift D
1–0	119.75	125.66	161.17	152.35
2–0	238.19	248.15	322.14	302.14
3–0	354.91	367.72	483.09	450.28
4–0	469.99	484.74	644.09	597.38
5–0	582.82	599.64	805.09	743.85
6–0	694.01	712.80	965.97	889.95
7–0	803.47	824.58	1126.58	1035.88
8–0	911.31	935.26	1286.75	1181.76
9–0	1017.67	1045.05	1446.34	1327.68
10–0	1122.69	1154.10	1605.23	1473.70

which supports our results.¹⁶ The geometry of CO₂ binding to the armchair nanotube shows the C=O bonding clearly across the Co–C bonding, while the zigzag shows a geometry of C=O of CO₂ parallel to the C–Co bonding, mainly for the SWNT(17,0)@Co. Therefore, a bidentate geometry leads to the largest binding energy. On the other hand, all interaction of CO₂ shows a direct binding of cobalt to the C of CO₂, thus yielding approximately the same equilibrium distances.

Figure 3 also makes clear the symmetry breaking of the CO₂ molecule under the influence of the Co atom. We can see that the CO₂ molecule loses its linear characteristic to display a bending angle ranging from 161 (armchair chirality) to 154° (zigzag chirality). This symmetry breaking for the CO₂ molecule is a strong indication of the greater interaction with SWNT@Co. Because no hybridization was observed to take place and the O–C–O bond angles are larger than the theoretical results of CO₂ complexed²⁶ with cobalt of 135° and a binding energy between 2.168 and 2.647 eV, we conclude that our results do not show a strictly chemical bonding of this CO₂ species.

Table 2 presents the equilibrium distance and binding energy for each SWNT@Co–CO₂. We note that while the equilibrium position is the same for the different SWNT@Co–CO₂ complexes, the binding energy values are quite different. The equilibrium position in this case must be considered to be the distance between the Co atom and the C atom of the molecule. The zigzag chirality presents a binding energy about two times larger than that of the armchair chirality. This table also shows that if we consider the diameter of the structures, the larger tube with armchair chirality has a higher binding energy, while the opposite occurs with the zigzag chirality.

Figure 4a presents the binding energy curves for the SWNT@Co–CO₂ interaction. These curves were obtained by maintaining the structures fixed and varying the distance between the CO₂ molecule and the cobalt atom from the asymptotic to the strongly interacting region. This picture strengthens the idea that the binding energy depends strongly on the chirality and is higher in the zigzag chirality. These

curves also indicate that the binding energy is inversely proportional to the diameter for zigzag and directly proportional for armchair. In Figure 4b, we also observed a huge difference between the energies of SWNT–CO₂ and SWNT@Co–CO₂. This fact was expected, considering that the addition of transition metals in SWNTs increases considerably the SWNT reactivity, as previously reported in the literature.¹³

In SWNT(5,5), we observe (see Figure 5) that charge superposition occurs exclusively between the Co atom and the carbon atom of the CO₂ molecule. In the case of SWNT(10,0), we note that the superposition of charge also involves an oxygen atom. This fact increases the binding energy between the Co and CO₂ molecule. When an armchair nanotube was considered, a carbon coordination complex was observed to take place, whereas the zigzag nanotube presents almost side-on coordination. The coordination of CO₂ to Co is mainly stabilized due to electrostatic and/or back-bonding interactions.²⁶ Morokuma and co-workers²⁶ showed that a side-on coordination requires a back-donation and electrostatic stabilization while carbon coordination is less favored, which supports our binding energy results. A slight bent coordination was found for the interaction with cobalt, which is in accordance with theoretical studies.²⁷ Theoretical study of CO₂ adsorption on cobalt surfaces shows a distance between 1.89 and 2.23 Å, which supports our results.¹⁶ Figure 6 shows the σ donation from the π orbital of CO₂ and π back-donation from the filled metal d orbital for Co–CO₂ interaction.

The density of states (DOS) for pristine and cobalt-doped nanotubes were also calculated. Figure 7 shows the electronic densities of states for these systems. The solid and dashed lines represent the DOS for pristine and cobalt-doped nanotubes, respectively. From Figure 7a, we observe that the Fermi levels for pristine and cobalt-doped nanotubes (5,5) are -4.67 and -5.05 eV, respectively. The same behavior occurs for the chirality (10,0) (Figure 7b) but with the Fermi level values equal to -4.23 and -5.29 eV, respectively. These Fermi level shifts are due to the Co atom, whose presence increases the amount of free electrons in the nanotube lattice and consequently favors the binding of the CO₂ molecule. This fact can also be observed by the increase in the number of states for the nanotube (5,5) and the emergence of states near the Fermi level for the nanotube (10,0).

After obtaining the single-point energies related to each inner dimer distance, we sought an analytical expression to accurately fit these energies. This is a fundamental step that allows us to solve the nuclear Schrödinger equation in order to obtain the vibrational and spectroscopic properties of the systems. In this sense, we take extra care in this fitting procedure by considering an extended Rydberg expression of degree 10 (see eq 1).

The aim is that, because this analytical expression reliably represented our energy values with a standard deviation smaller than 0.1 kcal/mol, we can accurately solve the nuclear Schrödinger equation for all considered regions of our

Table 7. Spectroscopic Constants for the SWNT–CO₂ Dimers

spectroscopic constants (cm ⁻¹)	SWNT(5,5)	SWNT(10,10)	SWNT(10,0)	SWNT(17,0)
ω_e	68.8967	65.6545	74.1150	66.6289
ω_{α_e}	1.8441	0.4166	1.7550	0.43636
$\omega_{\beta_e} \gamma_e$	0.0961	-0.0112	0.0186	-0.0317
α_e	0.0008	0.0009	0.0004	0.0004
γ_e	3.1078×10^{-5}	7.4167×10^{-5}	-2.3907×10^{-5}	-1.2187×10^{-5}

Table 8. Spectroscopic Constants for the SWNT@Co–CO₂ Dimers

spectroscopic constants (cm ⁻¹)	SWNT(5,5)@Co	SWNT(10,10)@Co	SWNT(10,0)@Co	SWNT(17,0)@Co
ω_e	189.6482	194.6163	235.6883	222.4148
$\omega_e \alpha_e$	2.2435	2.1261	2.0095	2.4034
$\omega_e \gamma_e$	0.0366	0.0110	0.0518	0.1209
α_e	0.0012	0.0010	0.0011	0.0014
γ_e	1.5473×10^{-5}	1.7768×10^{-6}	2.9448×10^{-5}	6.0973×10^{-5}

potential. Tables 3 and 4 summarize the fitting coefficients in eq 1 for the pristine and cobalt-doped dimers, respectively. The considerable difference in the coefficients is indicative of the aforementioned behavior of doping providing a great increase in binding energy. This comparison can be visualized in Figure 4, in which we consider a pristine and a cobalt-doped system on the same axes.

Once the analytical form for the potential is obtained considering the data from Tables 3 and 4, we can turn our attention to the solution of the nuclear Schrödinger equation for all of the systems of interest. Through this formalism, we investigate the vibrational spectra of the system and, as a consequence, the spectroscopic constants.

Table 5 presents the results of the first 10 vibrational states for the pristine and cobalt-doped dimers (values in parentheses). A remarkable fact observed is the higher values of the vibrational energies for the doped systems when compared with those of the pure SWNT. The electron transfer of back-bonding strengthen the Co–CO₂ bonding and should be related to the increase of this bonding vibration.

Table 6 shows the shift of the spectrum when the SWNT–CO₂ dimers are transferred from pristine to doped SWNT–CO₂. Shifts A, B, C, and D stand for SWNT(5,5)–CO₂ and SWNT(5,5)@Co–CO₂, SWNT(10,10)–CO₂ and SWNT(10,10)@Co–CO₂, SWNT(10,0)–CO₂ and SWNT(10,0)@Co–CO₂, and SWNT(17,0)–CO₂ and SWNT(17,0)@Co–CO₂, respectively. From this table, one can note that the red shifts are accompanied by a shortening of the SWNT@Co–CO₂ equilibrium distances (see Figures 2 and 4). These results mean that SWNT–CO₂ intermolecular interaction energies are weaker than those of SWNT@Co–CO₂ due to the interaction of the CO₂ molecule with Co and C atoms of the nanotube. The red shifts obtained belong to far and mid-infrared portions of the electromagnetic spectrum, as expected for intermolecular interactions.

Finally, by applying eq 2, we obtain the spectroscopic values for SWNT–CO₂ (Table 7) and SWNT@Co–CO₂ (Table 8) dimers. From these tables, it is possible to note that the SWNT@Co–CO₂ vibrational frequency constants, ω_e , are greater than ω_e for the SWNT–CO₂. These features show that in the SWNT@Co–CO₂ dimers, the frequencies are more harmonic than those for the SWNT–CO₂ dimers. The SWNT–CO₂ and SWNT@Co–CO₂ intermolecular rotation–vibration interaction constants (α_e and γ_e) are very small, which means that the rotational and vibrational modes are little coupled. These values are of major importance for future spectroscopic works and are to be used for comparison whenever experimental and theoretical studies on CO₂ adsorption on carbon nanotubes are considered.

4. CONCLUSIONS

In this work, we performed first-principles calculations to study the interaction of a molecule of CO₂ with the external surfaces of armchair (SWNT(5,5) and (10,10)) and zigzag (SWNT-

(10,10) and (17,0)) pristine and cobalt-doped carbon nanotubes in order to investigate the effects of doping, chirality, and diameter on the interaction process. We find that for pristine SWNTs, the CO₂ molecule of CO₂ interacts above the center of the hexagon on the surface of nanotubes, and the binding energy is about the same in all cases, independent of the diameter and the chirality considered. When we consider the interaction of the CO₂ molecule with the SWNT@Co, a considerable increase in binding energy for all cases covered was observed. We point out also that in this situation, the zigzag chirality shows higher values for the binding energy relative to armchair chirality. We also observed a direct relationship between the binding energy and the diameter of the nanotubes on armchair chirality and an inverse relationship in the case of zigzag chirality. Finally, the electron affinity between the CO₂ molecule and SWNT@Co suggests that the doping of carbon nanotubes with transition metals allows a good route to the construction of structures that can identify and capture this molecule in different environments.

AUTHOR INFORMATION

Notes

The authors declare no competing financial interest.

ACKNOWLEDGMENTS

The authors gratefully acknowledge the financial support from the Brazilian Research Councils CNPq, CAPES, and FINATEC.

REFERENCES

- Robert, G. W.; Erik, S. B.; Kare, L.; Curt, F. Photosynthesis of Submersed Macrophytes in Acidified Lakes II. Carbon Limitation and Utilization of Benthic CO₂ Sources. *Aquat. Bot.* **1985**, *22*, 107.
- Charles, E.; Murphy, Jr. Carbon Dioxide Exchange and Growth of a Pine Plantation. *For. Ecol. Manage.* **1985**, *11*, 203.
- Chaudhuri, U. N.; Burnett, R. B.; Kirkham, M. B.; Kanemasu, E. T. Effect of Carbon Dioxide on Sorghum Yield, Root Growth, and Water Use. *Agric. For. Meteorol.* **1986**, *37*, 109.
- Mantripragada, H. C.; Rubin, E. S. Techno-economic Evaluation of Coal-to-Liquids (CTL) Plants With Carbon Capture and Sequestration. *Energy Policy* **2011**, *39*, 2808.
- Montzka, S. A.; Dlugokencky, E. J.; Butler, J. H. Non-CO₂ Greenhouse Gases and Climate Change. *Nature* **2011**, *476*, 43.
- Hopkins, F. E.; Turner, S. M.; Nightingale, P. D.; Steinke, M.; Bakker, D.; Liss, P. S. Ocean Acidification and Marine Trace Gas Emissions. *Proc. Natl. Acad. Sci. U.S.A.* **2010**, *107*, 760.
- Ebbesen, T. W. *Carbon Nanotubes: Preparation and Properties*; CRC: Boca Raton, FL, 1997.
- Saito, R.; Dresselhaus, G.; Dresselhaus, M. S. *Physical Properties of Carbon Nanotubes*; Imperial College Press: London, 2003.
- Carbon Nanotubes: Applications on Electron Devices*; Marulanda, J. M., Ed.; InTech: Rijeka, Croatia, 2011.
- Hierold, C. *Carbon Nanotube Devices: Properties, Modeling, Integration and Applications*; Wiley-VCH: Weinheim, Germany, 2008.

- (11) Zhao, J.; Buldum, A.; Han, J.; Lu, J. P. Gas Molecule Adsorption in Carbon Nanotubes and Nanotube Bundles. *Nanotechnology* **2002**, *13*, 195.
- (12) Cinke, M.; Li, J.; Bauschlicher, C. W.; Ricca, A.; Meyyappan, M. CO₂ Adsorption in Single-Walled Carbon Nanotubes. *Chem. Phys. Lett.* **2003**, *376*, 761.
- (13) Garcia-Lastra, J. M.; Mowbray, D. J.; Thygesen, K. S.; Rubio, A.; Jacobsen, K. W. Modeling Nanoscale Gas Sensors Under Realistic Conditions: Computational Screening of Metal-Doped Carbon Nanotubes. *Phys. Rev. B* **2010**, *81*, 245429/1–.
- (14) Matranga, C.; Bockrath, B. Permanent Trapping of CO₂ in Single-Walled Carbon Nanotubes Synthesized by the HiPco Process. *J. Phys. Chem. B* **2004**, *108*, 6170.
- (15) Fujita, E.; Furenlid, L. R.; Renner, M. W. Direct XANES Evidence for Charge Transfer in CoCO₂ Complexes. *J. Am. Chem. Soc.* **1997**, *119*, 4549.
- (16) De la Peña O’Shea, V. A.; González, S.; Illas, F.; Fierro, J. L. G. Evidence for Spontaneous CO₂ Activation on Cobalt Surfaces. *Chem. Phys. Lett.* **2008**, *454*, 262.
- (17) Szalda, D. J.; Chou, M. H.; Fujita, E.; Creutz, C. Properties and Reactivity of Metallocarboxylates. Crystal and Molecular Structure of the $-CO_2^{2-}$ -Bridged “Polymer” $[Co^{III}(en)_2(CO_2)](ClO_4).H_2O]_n$. *Inorg. Chem.* **1992**, *31*, 4712.
- (18) Gibson, D. H.; Ye, M.; Richardson, J. F. Synthesis and Characterization of $\mu_2\eta^2$ - and $\mu_2\eta^3$ -CO₂ Complexes of Iron and Rhodium. *J. Am. Chem. Soc.* **1992**, *114*, 9716.
- (19) Accelrys Software Inc. *Discovery Studio Modeling Environment*, Release 3.5; Accelrys Software Inc.: San Diego, CA, 2012.
- (20) Perdew, J. P.; Wang, Y. Accurate and Simple Analytic Representation of the Electron–Gas Correlation Energy. *Phys. Rev. B* **1992**, *45*, 13244.
- (21) Murrell, J. N.; Carter, S.; Farantos, S. C.; Huxley, P.; Varandas, A. J. C. *Molecular Potential Energy Functions*; Wiley: Chichester, U.K., 1984.
- (22) Powell, M. J. D. An Efficient Method for Finding the Minimum of a Function of Several Variables Without Calculating Derivatives. *Comput. J.* **1964**, *2*, 155.
- (23) Neto, J. J. S.; Costa, L. S. Numerical Generation of Optimized Discrete Variable Representations. *Braz. J. Phys.* **1998**, *111*, 28.
- (24) Vila, H. V. R.; Leal, L. A.; Ribeiro, L. A.; Martins, J. B. L.; E Silva, G. M.; Gargano, R. Spectroscopic Properties of the Molecular Ion in the 8k π , 9k σ , 9l π , 9l σ and 10o σ Electronic States. *J. Mol. Spectrosc.* **2012**, *273*, 26.
- (25) Vidali, G.; Ihm, G.; Kim, H. Y.; Cole, M. W. Potentials of Physical Adsorption. *Surf. Sci. Rep.* **1991**, *12*, 181.
- (26) Sakaki, S.; Kitaura, K.; Morokuma, K. Structure and Coordinate Bonding Nature of Nickel(0) and Copper(I) Carbon Dioxide Complexes. An ab initio Molecular Orbital Study. *Inorg. Chem.* **1982**, *21*, 160.
- (27) Freund, H. J.; Roberts, M. W. Surface Chemistry of Carbon Dioxide. *Surf. Sci. Rep.* **1996**, *25*, 225.